Hindawi
International Journal of Aerospace Engineering
Volume 2019, Article ID 8513149, 10 pages
https://doi.org/10.1155/2019/8513149

Research Article

Effect of Gravity on Repose Angle and Contact Forces of Particulate Pile Composed of Non-monodispersed Particles

H. Chen,[1] **Y. X. Chen**,[2] **Q. S. Wei**,[1] **and Y. S. Shi**[1]

[1]*School of Materials Science and Engineering, Huazhong University of Science and Technology, Wuhan 430074, China*
[2]*CCCC Rail Transit Consultants Co. Ltd, Wuhan branch, Wuhan 430056, China*

Correspondence should be addressed to Q. S. Wei; wqs_xn@hust.edu.cn

Received 21 May 2018; Revised 13 October 2018; Accepted 31 October 2018; Published 4 February 2019

Academic Editor: Yue Wang

Evaluating the repose angle of granular materials under different kinds of gravitational conditions is essential for in situ resource exploration on surfaces of other Earth-like planets in the next decades. The forming process of particulate pile under different kinds of gravitational accelerations was simulated by three-dimensional discrete element method (DEM), where the particulate piles composed of normally distributed particles and lognormally distributed particles were considered, respectively. The effects of gravity on the repose angle and contact forces of the particulate pile were investigated. The results show that, for particulate pile composed of normally or lognormally distributed particles, the effect of gravity force on the repose angle is ignorable. For particles with a certain kind of size distribution, the distribution functions of normalized contact forces in the particulate pile under different gravity accelerations show to be in mutual coincidence. No obvious effect of the particle size distribution on the relation between the gravity acceleration and repose angle is observed.

1. Introduction

Repose angle, the maximum slope angle at which the material is at rest, is a basic and important property of granular materials [1, 2]. The forming of repose angle is a bulk flow behavior of particle system, depending on the collective interactions of individual particles. Above this angle, the material begins to flow; below this angle, the material is stable. The repose angle is an empirical friction parameter that is essential in the models of numerous phenomena involving granular material, most of them actually at slopes close to the repose angle [3, 4]. Therefore, the repose angle of granular materials is relevant for many geomorphological phenomena [5, 6].

Gravity is the determinant driving force in the forming of repose angle for granular materials, but the correlation of gravitational strength and repose angle is hardly investigated and not well understood. The repose angle that is resulted from the particulate flow driven by gravity is extremely significant in the understanding of the surface geological environment of terrestrial planets, which will be valuable for human in situ exploration and building on the surfaces of the Moon or Mars in the near future. For instance, the surface morphologic features on Earth-like planets such as Mars and Moon are thought to be resulted from the avalanches of loose granules [7–9]. Meanwhile, the landing and traveling of exploration vehicles on the surface of loose particulate materials will be needed in the explorations on planets such as Moon and Mars for the in situ excavation and collection of surface resources [10]. As gravitation strength varies on different kinds of terrestrial planets, the correlation between gravity and repose angle of loose granules, therefore, is particularly important to clarify the geology conditions of various kinds of planets and to evaluate the environments which might be encountered in the planet explorations.

Until now, the correlation between the gravitation and repose angle of granular materials is still unclear. Although some researchers have been conducted to study about this issue, results from those literatures conflict with each other. For example, the parabolic flight method was employed by Kleinhans et al. [11] to produce low gravity conditions, where the formations of pile were conducted for different kinds of

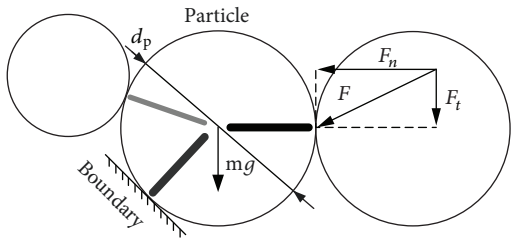

Figure 1: Force diagram of individual particles in DEM model.

particulate materials, respectively. They pointed out that the repose angle of particles under lunar gravity condition could be increased by about 5°. However, Nakashima et al. [12] conducted experimental tests similar to the work of Kleinhans et al. [11] but proposed that the function of gravity force on the repose angle of particulate pile was negligible. Hofmeister et al. [13] conducted a study about this issue where the repose angle was tested in a centrifuge and a dropping tower, respectively. Their tests pointed out that the repose angle of particles would increase with the decreasing of gravity strength. In the study of Atwood-Stone and McEwen [14], they used a high-resolution-imaging method (HRI) to test the repose angle of packed sand dunes on the surface of Mars, where no obvious effect of gravity on the repose angle was observed. In the studies of Ji and Shen [15], the forming process of particulate piles under gravity with different kinds of strength was simulated with 2D discrete element method. And they believed that the repose angle of particulate materials was not correlated to the strength of gravity, at least for the gravity condition ranging from 1/6 to 1 times of gravitational acceleration on Earth.

We recently carried out a numerical study on the forming of particulate pile composed of monodispersed particles under variable gravitations based on three-dimensional discrete element method (DEM) [16], where the correlation between the gravity and repose angle was evaluated. However, the sizes of granular solids are commonly not monodispersed, no matter on the surface of the Earth or other Earth-like planets. This paper extends that work by investigating the forming process of particulate pile composed of non-monodispersed particles under different gravitational conditions. The effects of gravity force on the repose angle of particulate pile and contact force within it were investigated. The results obtained would be useful for our further understanding about the formation of particulate pile under different kinds of gravitations.

2. Methods

2.1. Governing Equations for Particle. The discrete element method (DEM) with soft contact model proposed by Cundall and Strack [17] was employed to simulate the formation particulate piles under variable gravitational conditions. Figure 1 sketched the force diagram of individual particle with size of $\mathbf{d}_p$ in DEM model, where F_n and F_t are, respectively, the normal and tangential contact forces on the particle, accounting for the particle-particle and particle-boundary interactions; m$\mathbf{g}$ is the gravitational force of the particle. Besides, virtual links between the particle contact points and particle centres [18] were considered as the force networks within the particulate system. As shown in the figure, each connection between two individual particles will be represented by a bar with its colour depth proportional to the magnitude of the contact force. For the particle i in the granular system, the translational and rotational motions with time t are solved by Newton's second law of motion, which is given by

$$m_i \frac{\mathrm{d}^2 \mathbf{r}_i}{\mathrm{d}t^2} = m_i \mathbf{g} + \sum_j \left(F_{\mathrm{n},ij} + F_{\mathrm{t},ij}\right), \tag{1}$$

$$I_i \frac{\mathrm{d}^2 \boldsymbol{\theta}_i}{\mathrm{d}t^2} = \sum_j T_{ij} = \sum_j \left(\mathbf{R}_i \times F_{\mathrm{t},ij} - \mu_{\mathrm{r},ij} R_i F_{\mathrm{n},ij} \dot{\boldsymbol{\theta}}_i\right), \tag{2}$$

where m_i, R_i, I_i, $\mathbf{r}_i$, and $\boldsymbol{\theta}_i$ are, respectively, the mass, radius, moment of inertia, position vector, and angular displacement of particle i; $F_{\mathrm{n},ij}$, $F_{\mathrm{t},ij}$, and T_{ij} are, respectively, the normal contact force, tangential contact force, and moment on particle i, resulting from the contact of particle i with particle j; $\mu_{\mathrm{r},ij}$ is the rolling friction coefficient between particle i and j; and $\mathbf{g}$ is the gravity acceleration of particle i.

Currently, there are three basic contact force models for elastic-plastic collisions at single particle impact scale [17, 19]: Hertz-Mindlin model, simplified Hertz-Mindlin model, and linearly contact model. The Hertz-Mindlin model has been employed in our previous research about this issue [16]. The linear model was in close agreement with Hertz-Mindlin model and even outperformed some of the other more complex models. On this basis, the linear model is employed in the current work for its simplicity in order to reduce computational complexity. Then, the normal and tangential contact forces, $F_{\mathrm{n},ij}$ and $F_{\mathrm{t},ij}$, in equations (1) and (2) are given by

$$F_{\mathrm{n},ij} = k_\mathrm{n} \boldsymbol{\delta}_\mathrm{n} + c_\mathrm{n} \dot{\boldsymbol{\delta}}_\mathrm{n}, \tag{3}$$

$$F_{\mathrm{t},ij} = \min\left(k_\mathrm{t} \boldsymbol{\delta}_\mathrm{t} + c_\mathrm{t} \dot{\boldsymbol{\delta}}_\mathrm{t}, \mu_\mathrm{s} \left|F_{\mathrm{n},ij}\right|\right), \tag{4}$$

where k_n and c_n are, respectively, the stiffness coefficient and damping coefficient in the normal direction; k_t and c_t are, respectively, the stiffness coefficient and damping coefficient in the tangential direction; μ_s is the sliding friction coefficient between particles; $\boldsymbol{\delta}_\mathrm{n}$ and $\boldsymbol{\delta}_\mathrm{t}$ are, respectively, the normal and tangential displacements between particle i and j.

The parameters k_t and c_t related to the real mechanical properties can, respectively, be assumed equal to k_n and c_n in linear model [20], and they can be described as functions of material parameters of the particle according to the Hertz contact theory:

$$\begin{aligned} k_\mathrm{n} &= \frac{16}{15} R^{*1/2} E^* \left(\frac{15 m^* \sigma_i^2}{16 R^{*1/2} E^*}\right)^{1/5}, \\ c_\mathrm{n} &= \left(\frac{4 m^* k_\mathrm{n}}{1 + \left(\pi / \ln e_{ij}\right)^2}\right)^{1/2}, \end{aligned} \tag{5}$$

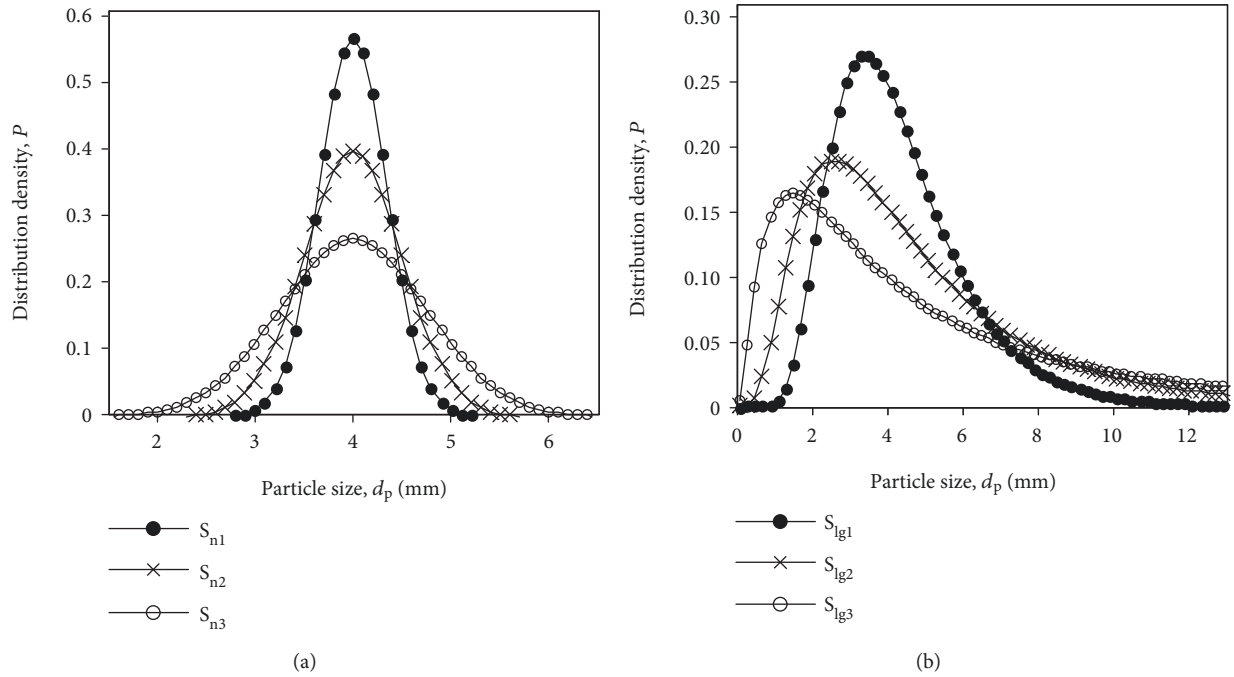

FIGURE 2: Size distributions of particle samples: (a) samples S_{n1}, S_{n2}, and S_{n3} with normal distributions and (b) samples S_{lg1}, S_{lg2}, and S_{lg3} with lognormal distributions.

where R^*, m^*, and E^* are the equivalent particle properties which can be calculated in terms of the real particle properties, respectively $(R^* = R_iR_j/(R_i + R_j)$, $m^* = m_im_j/(m_i + m_j)$, and $E^* = E_iE_j/[(1-\sigma_j^2)E_i + (1-\sigma_i^2)E_j]$, where R_i, m_i, and E_i are, respectively, the radius, mass, and Young's modulus of particle i; R_j, m_j, and E_j are, respectively, the radius, mass, and Young's modulus of particle j); σ_i and σ_j are the Poisson's ratio of particle i and j, respectively; and e_{ij} is the restitution coefficient between particle i and j.

Additionally, the normal and tangential relative velocities between particle i and j, $\dot{\boldsymbol{\delta}}_n$ and $\dot{\boldsymbol{\delta}}_t$, are the functions of the position vector $\mathbf{r}$, angular displacement $\boldsymbol{\theta}$, and radius $\mathbf{R}$ of particles:

$$\begin{aligned}\dot{\boldsymbol{\delta}}_n &= \left(\dot{\mathbf{r}}_i - \dot{\mathbf{r}}_j\right)\cdot\mathbf{n},\\ \dot{\boldsymbol{\delta}}_t &= \left(\dot{\mathbf{r}}_i - \dot{\mathbf{r}}_j + \mathbf{R}_i\times\dot{\boldsymbol{\theta}}_i + \mathbf{R}_j\times\dot{\boldsymbol{\theta}}_j\right)\times\mathbf{n},\end{aligned} \tag{6}$$

where the normal unit vector $\mathbf{n}$ is described as $\mathbf{n} = (r_i - r_j)/|r_i - r_j|$. By the integration of $\dot{\boldsymbol{\delta}}_t$ and $\dot{\boldsymbol{\delta}}_n$, the tangential displacement $\boldsymbol{\delta}_t$ and normal displacement $\boldsymbol{\delta}_n$ between individual particles in equations (3) and (4) can be obtained, respectively.

In the model, the program module for calculating $F_{n,ij}$ and $F_{t,ij}$ is available only when the contact between particles occurs, which is given by

$$\left|\mathbf{r}_i - \mathbf{r}_j\right| < R_i + R_j. \tag{7}$$

The time step $\triangle t$ should be smaller than the characteristic time τ_c, which corresponds to a typical contact time between two colliding particles [17]:

$$\Delta t \le \tau_c = \frac{\pi\bar{R}}{\varepsilon}\sqrt{\frac{\rho}{G}}, \tag{8}$$

where ρ is the particle density; $\bar{R}$ is the average particle radius; and $G = E/2(1+\sigma)$ is the particle shear modulus. ε can be obtained from [21]

$$\left(2-\varepsilon^2\right)^4 = 16\left(1-\varepsilon^2\right)\left[1-\varepsilon^2\frac{1-2\sigma}{2(1-\sigma)}\right], \tag{9}$$

which can be approximated by

$$\varepsilon = 0.8766 + 0.163\sigma. \tag{10}$$

The appropriate time step for calculating the particle motion equations in dense particulate systems ranges from 20% to 80% of τ_c [21]. In this work, considering both of the computation accuracy and costs, the time step for DEM calculation was set to be 50% of τ_c. Moreover, the computational domain was decomposed into subdomains to reduce the real CPU costs, and the code was run in parallel on our Dell T7810 workstation, with 32 concurrent execution threads.

2.2. Simulation Conditions. In normal conditions, granular materials on the surface of the Earth or other planets are not monodispersed in particle size. The commonly size

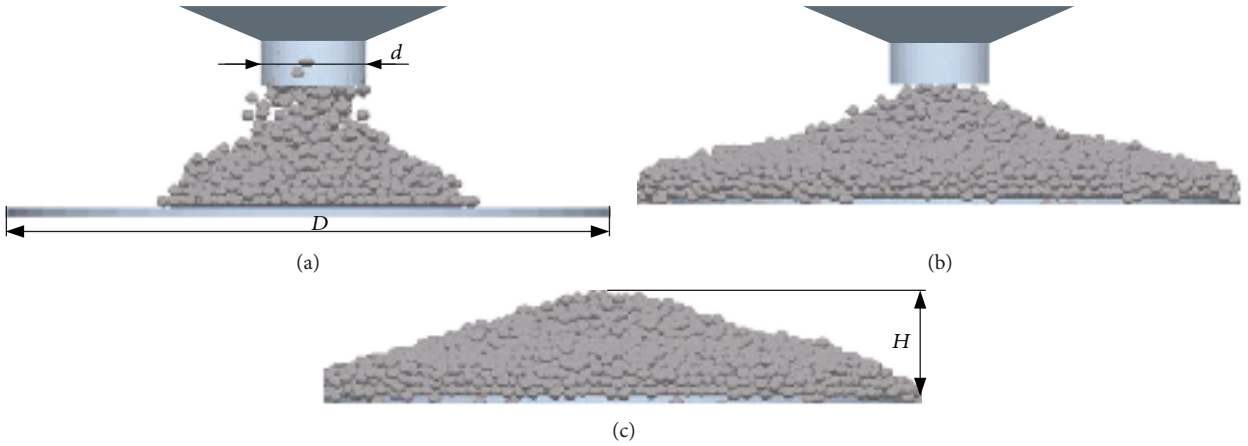

Figure 3: Formation of particulate pile in our DEM simulations: (a) beginning of the particle accumulation, (b) accumulation saturated, and (c) packed particulate pile.

distribution of granular materials in nature world is normal distribution or lognormal distribution. Six kinds of particle samples were considered in the DEM model: sample S_{n1}, S_{n2}, and S_{n3} with different kinds of normal distribution in particle size, as shown in Figure 2(a); sample S_{lg1}, S_{lg2}, and S_{lg3} with different kinds of lognormal distribution in particle size, as shown in Figure 2(b). Note that the expectancy value of particle size for all the samples is 4 mm.

As shown in Figure 3, the point-source dropping method [16, 20] was used to produce the particulate pile packed on a baseplate in our simulations. The baseplate was considered as a special particle with infinite mass following the motion of equation (1) and equation (2). As shown in Figure 3(a), at the beginning of the DEM simulation, a horizontally placed circular baseplate was set as the boundary for particle motions, where D was the diameter of the baseplate. And a hopper was set above the centre of the baseplate, where d was the diameter of the outlet. Particles were continuously generated and filled in the hopper. As shown in Figure 3(b), particles are unloaded from the hopper, dropped onto the centre of the baseplate, and piled up gradually on the baseplate, owing to the action of gravity force. As shown in Figure 3(c), the emulation of the model would be stopped until a particulate pile was fully packed on the baseplate, where H is the height of the packed particle pile. Then the discharge outlet of the funnel was closed, and the simulation would continue until the granular pile became stable. For all cases of our simulations, the iteration of particle motion equations will be stopped when the velocity of all particles is no more than 0.1 mm/s. And then it was considered that the static state of the powder pile was achieved. The repose angle of the pile can be calculated as a function of the pile height H and baseplate diameter D, which is given by

$$\alpha = \frac{180}{\pi} \times \arctan\left(\frac{2H}{D}\right). \tag{11}$$

The material properties of particle sample and baseplate were supposed to be glass and steel, which had been used in our previous work [16], as shown in Table 1. Note that, in the model, the sliding and rolling friction coefficients of particle-baseplate are set larger than that of particle-particle in order to ensure the forming of particulate pile on the surface of the baseplate.

Table 1: Parameters used in the model.

Properties	Value
Density of particle, ρ	2500 kg/m^3
Young's modulus of particle, E_p	5.5×10^9 Pa
Young's modulus of baseplate, E_b	2×10^9 Pa
Poisson's ratio of particle, σ_p	0.24
Poisson's ratio of baseplate, σ_b	0.3
Restitution coefficient of particle-particle, e_{pp}	0.97
Restitution coefficient of particle-baseplate, e_{pb}	0.97
Diameter of baseplate, D	500 mm
Diameter of discharge outlet, d	50 mm
Sliding friction coefficient of particle-particle, $\mu_{t\text{-}pp}$	0.142
Rolling friction coefficient of particle-particle, $\mu_{r\text{-}pp}$	0.01
Sliding friction coefficient of particle-baseplate, $\mu_{s\text{-}pb}$	1.2
Rolling friction coefficient of particle-baseplate, $\mu_{r\text{-}pb}$	0.6
Acceleration of gravity, g	$0.17g_0$, $0.44g_0$, g_0, $3g_0$

Four kinds of gravity accelerations will be used for the formation of particulate pile in our DEM simulations: $0.17g_0$, $0.44g_0$, g_0, and $3g_0$, respectively, where g_0 is the gravity acceleration on Earth.

3. Results and Discussion

3.1. Particulate Pile under Variable g. For the particle sample S_{n1} with normal size distribution (see Figure 2), the profiles of the particulate pile formed under the four kinds of gravity

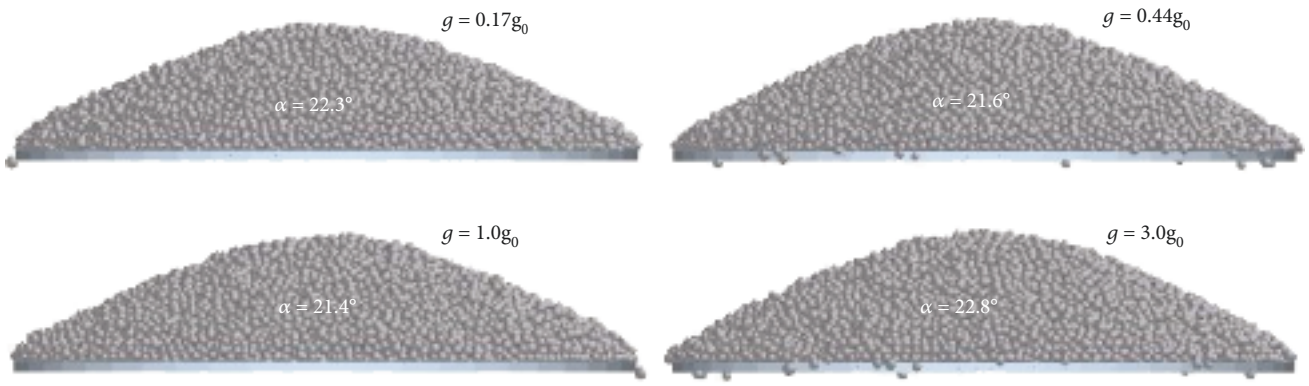

FIGURE 4: Particulate pile under different gravity conditions for particle sample S_{n1}.

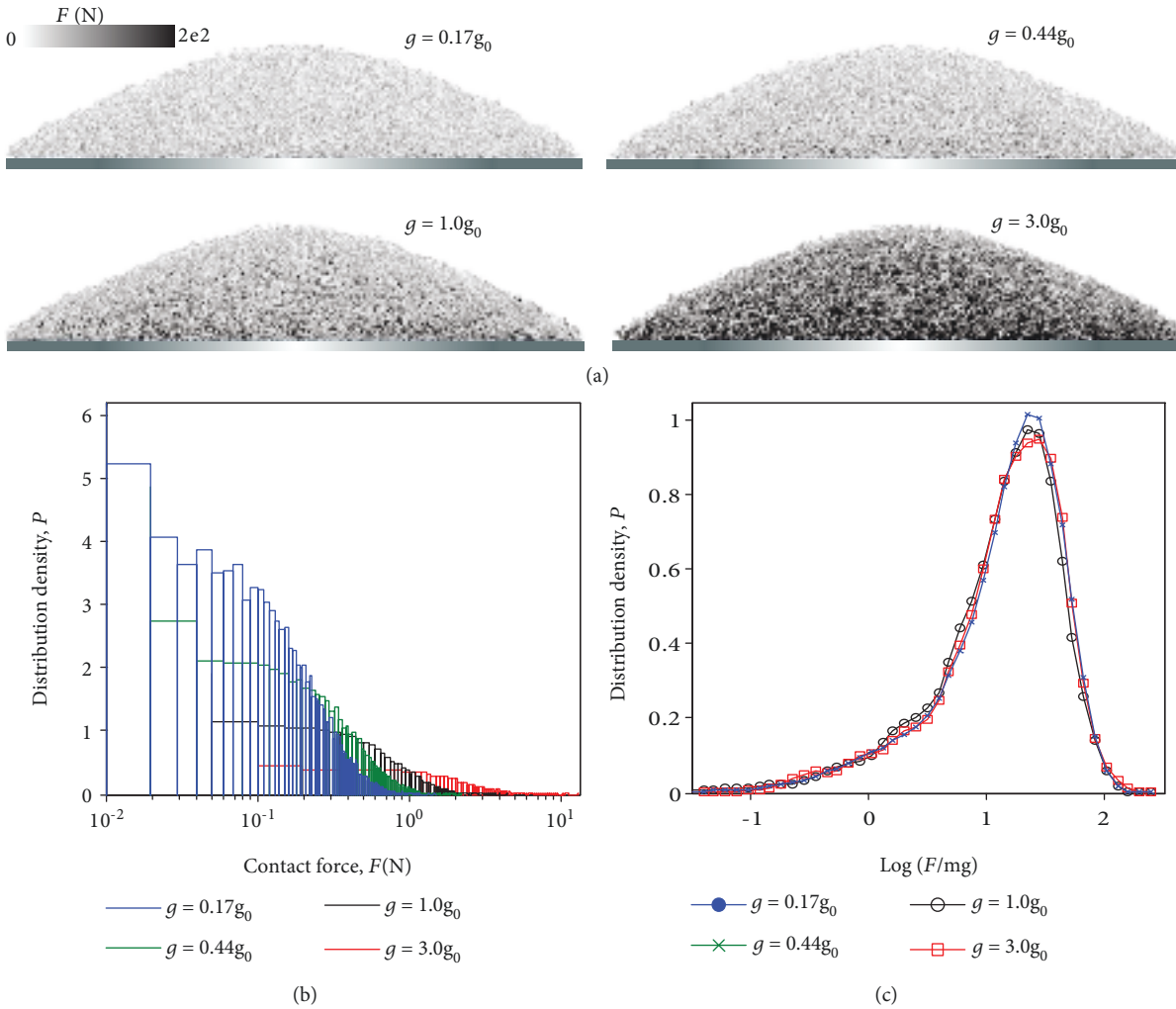

FIGURE 5: Contact force within particulate piles formed under different kinds of gravity accelerations for sample S_{n1}: (a) morphology of force networks, (b) distribution function of contact forces, and (c) distribution function of normalized contact forces.

accelerations are, respectively, plotted in Figure 4. As seen in the figure, no obvious variation occurs to the macroscopical profile of the pile when the strength of the gravity changes, although some local differences exist between the piles due to the random motion of individual particles during the formation process. The variation of repose angle calculated according to equation (11) is no more than 1° when the gravity changes from $0.17g_0$ to $3g_0$. So it comes to the conclusion that the effect of the gravity strength on the repose angle of pile is negligible. This law agrees with the particulate pile composed of monodispersed particles [15, 16].

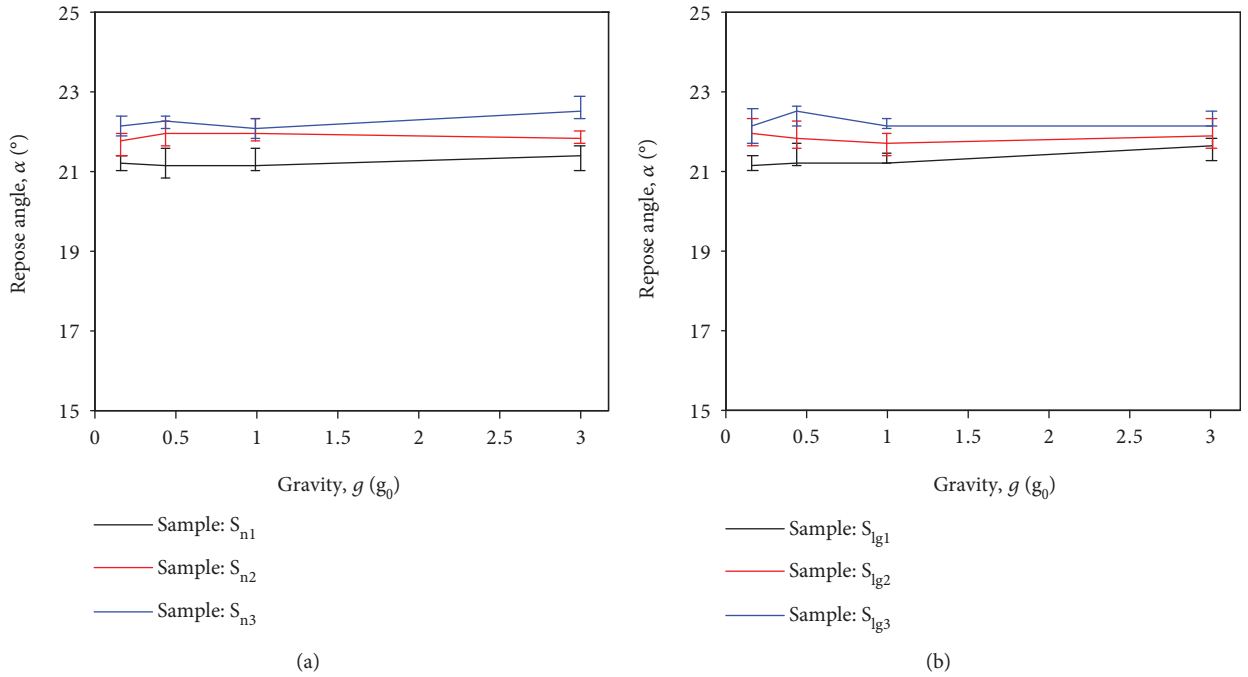

Figure 6: Repose angle of particulate pile under different gravity conditions for (a) particle samples with normal size distributions and (b) particle samples with lognormal size distributions.

For the particulate pile illustrated in Figure 4, the corresponding contact forces between particles within them are plotted in Figure 5. Based on the morphology of the contact-force networks in the piles, as plotted in Figure 5(a), it can be found that the strength of the contact forces within the particulate pile increases when the gravity acceleration increases. The local structures of the force network in the piles differ from each other when the gravity acceleration changes. Figure 5(b) shows the probability distribution functions of contact forces within the piles for different kinds of gravity strength. As seen in the figure, the strength of contact forces increases to a larger magnitude when the gravity acceleration increases. Similar to the condition of pile composed of monodispersed particles [16], the distribution function of contact forces for sample S_{n1} also has a similar shape under different kinds of gravitational strengths, and these distribution functions could be collapsed by just one curve. Then, the distribution functions of contact forces under different kinds of gravitational accelerations are plotted in Figure 5(c), where the contact forces are presented in dimensionless form, i.e., normalized by the average value of particle gravity in corresponding pile. As seen in the figure, the dimensionless distribution functions under variable gravity accelerations can be nearly fitted by one curve equation. It means that, from the view of statistics, the strength of the contact forces in the particulate pile is linearly proportional to the strength of the gravitational acceleration. Therefore, the distribution law of contact force for monodispersed particles [16] is also followed by the normally distributed particles.

The size distribution of particles is an important factor related to the repose angle [2, 4, 20], which might affect the correlation between the repose angle and gravity acceleration. To assess this problem, the formation of particulate pile under different gravity accelerations was performed for the six kinds of particle samples, respectively. Figure 6 shows the repose angle of particulate pile for all particle samples under the four kinds of gravitational accelerations, respectively. As can be seen in the figure, the repose angles are different from each other among the particle samples due to the differences of particle size distributions. However, the correlation between the repose angle and size distribution of particles is not the emphasis of this work and will not be discussed in detail. The focus in Figure 6 is that, for a given kind of particle sample, no significant variations occur to the repose angle of the pile when the gravity increases from $0.17g_0$ to $3g_0$, suggesting that the repose angle is independent of the strength of gravity no matter for particles with normal size distributions or lognormal size distributions. Therefore, the conclusion can be made that the effect of gravity strength on the repose angle of particulate pile is negligible, and this law will not be affected by the size distribution of particles.

3.2. Contact Forces of Particulate Pile. Figure 7 shows the effect of gravity acceleration on the probability distribution function of contact force within the pile for the six kinds of particle samples, respectively. Note that the contact forces are, respectively, normalized by the average particle weight in the corresponding pile. As shown in the figure, for a given kind of particle sample, the distribution functions of contact forces under the four kinds of gravity accelerations almost overlapped with each other. As the contact forces are normalized by the gravity acceleration, it means that, from the view of statistics, the contact forces within the particulate pile increase linearly with the strength of gravitational

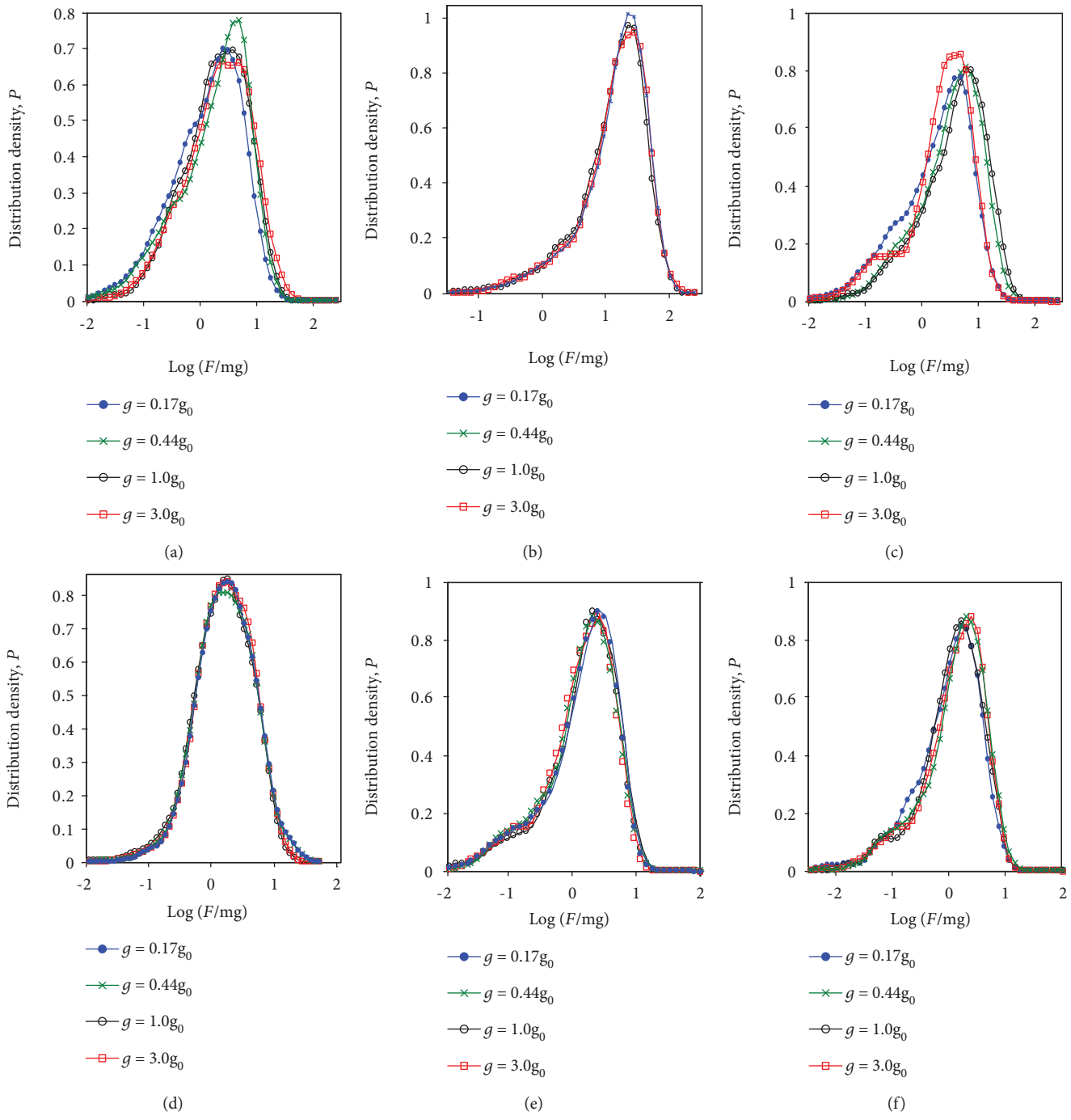

FIGURE 7: Probability distributions of contact force F in the particulate pile under different kinds of gravity accelerations for particle samples: (a) S_{n1}, (b) S_{n2}, (c) S_{n3}, (d) S_{lg1}, (e) S_{lg2}, and (f) S_{lg3}.

acceleration, no matter for the particles following the normal size distributions or lognormal size distributions. On the basis of the results from monodispersed particles [16], it can be concluded that the contact forces in the particulate pile scale linearly with the strength of gravitational acceleration, which is not influenced by the size distributions of particles.

The contact force F at each contact point between particles, as sketched in Figure 1, involves the tangential component F_t and normal component F_n. We define η as the ratio between tangential and normal contact forces at each contact point, which is given by

$$\eta = \frac{F_{t,ij}}{F_{n,ij}}. \tag{12}$$

Then, the probability distributions of η for contact points within particulate pile under different kinds of gravity accelerations are plotted in Figure 8 for the six kinds of particle

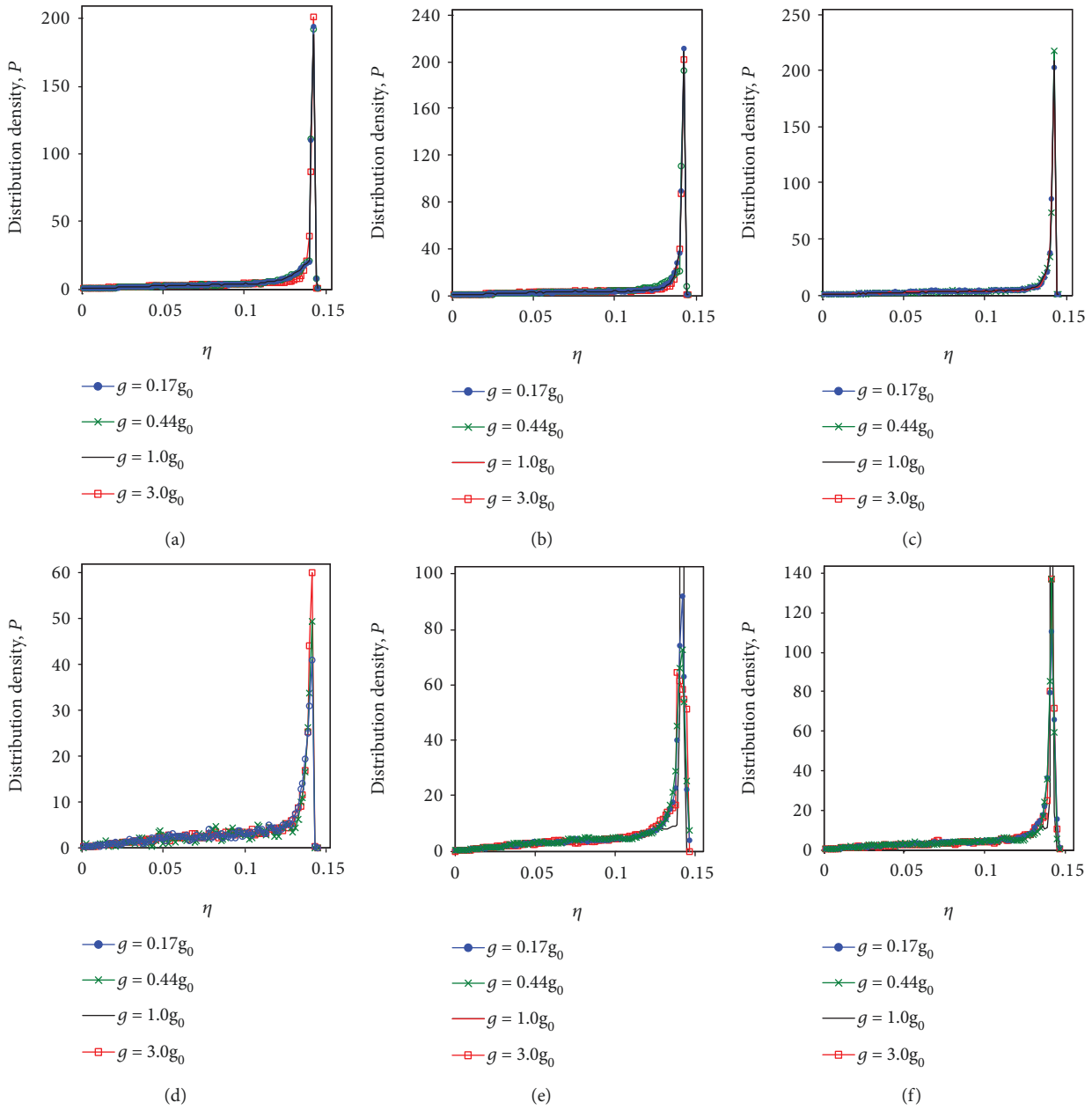

FIGURE 8: Probability distributions of η ($\eta = F_t/F_n$) in the particulate pile under different gravity accelerations for particle sample: (a) S_{n1}, (b) S_{n2}, (c) S_{n3}, (d) S_{lg1}, (e) S_{lg2}, and (f) S_{lg3}.

samples, respectively. As shown in the figure, the distribution functions of η for the six kinds of particle samples differ from each other. However, the emphasis in this work is that the distribution functions of η under different kinds of gravity accelerations can be nearly collapsed into one curve for a given kind of particle sample with normal size distribution or lognormal size distribution. It suggests that, for the contact points within a particulate pile, the ratio between the tangential and normal contact forces is independent of the gravity acceleration, and this phenomenon is not influenced by the size distribution of particles.

3.3. Discussions. From the mechanical equilibrium of a single particulate solid on a slope face, as sketched in Figure 9(a), the repose angle can be simply considered as the minimum slope angle where the particle can move downslope. This slope angle can be determined when the component of the particle weight along the slope direction is no more than the friction force acting on the particles on the slope surface [12]. When examining the equilibrium equation of the repose angle, it is easy to understand that the magnitude of gravity is irrelevant to the repose angle, as the gravity term for both the tangential and normal forces is identical and thus cancels out of the equation entirely. However, as sketched in Figure 9(b), the repose angle is the collective interactions of a cluster of individual particles, where the force equilibrium principle for a single particle (Figure 9(a)) is not applicable. Theoretically speaking, the whole contact-

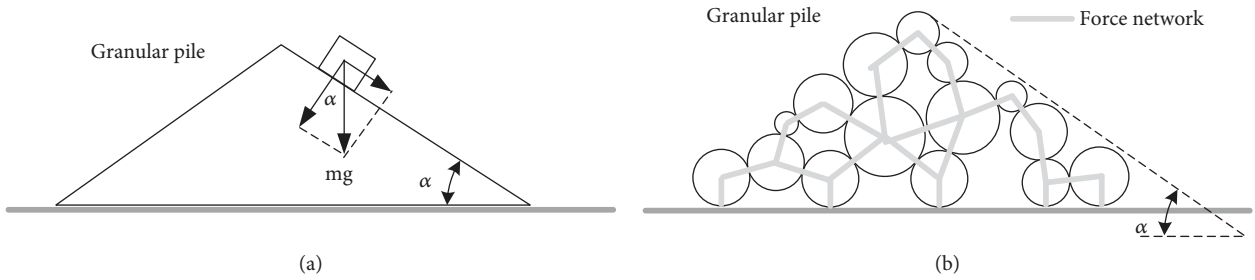

Figure 9: Force diagram of repose angle for (a) single particulate solid and (b) a cluster of particles.

force network in the particulate pile should keep in force balance and thus can support the particulate pile with a certain value of repose angle. The necessary and sufficient condition to keep the force network in balance is that all the contact points in the pile should be in mechanical equilibrium. It is difficult or even impossible to compare each contact force in the pile under different gravitational cases, as the local structure of the contact-force network in pile varies randomly in each case. In this work, therefore, the contact forces in the particulate pile under different gravitational accelerations were investigated statistically. Then, from the statistics view, the strength of contact forces within a particulate pile is linearly proportional to the gravity acceleration (Figure 7), and the ratio between the tangential and normal contact force at the contact points will not be influenced by the gravitational acceleration (Figure 8) for all the powder samples with normal size distributions or lognormal size distributions. It seems that when the gravity acceleration changes, the forces at contact points in the particulate pile just have changes in magnitudes but not in directions. Therefore, the force balance for all contact points in the pile will not be broken by the variation of gravitational acceleration, and thus the whole force networks supporting the pile with a certain repose angle can keep in balance. That is why the repose angle of particulate pile does not change when the strength of gravity acceleration varies. Combined with our study for monosized particles, we can speculate that the mechanical balance of the contact-force network, which supports the particulate pile and determines the repose angle, is not affected by the strength of gravity acceleration. This might be a basic law underlying the formation of particulate pile which is independent to the particle size distributions. Besides, the specific values of contact forces within the granular pile, which can be expected, are correlated with the contact model employed in the DEM simulation. In our previous DEM simulations, the contact model used to calculate the contact forces between particles is Hertz-Mindlin model. In this work, however, the same conclusion that the repose angle is not affected by the gravity strength is still obtained, with the linear model. So, we proposed that the contact force model between particles plays an ignorable role in the relationship between the repose angle and gravity.

For non-monosized particles which are normally distributed or lognormally distributed, our results still agree with the viewpoint that the repose angle is independent of the strength of gravity. We speculate that the repose angle of particulate pile is an inherence of granular materials just related to physical properties of particles but independent of the strength of gravity, although gravity is the original driving force leading to the repose angle of particulate pile. Recently, the assumption that the repose angle increases with the decreasing of gravity has been used by some researches [10] to evaluate the forming processes of dune gullies on the surface of Mars. If the results in this paper can be validated by in situ experiments, then many such works and discussions will need to be revisited. However, it should be noted that our conclusion is obtained in an ideal condition, where the interaction forces between granular particles considered in the numerical model are just the pure contact force resulted from elastic-plastic deformations. Under actually conditions, other interaction forces such as cohesion forces, liquid-bridge forces, and electrostatic forces might exist in some granular materials. These kinds of interaction forces can influence the repose angle of granular pile greatly and are coupled with the gravity force [22]. In such conditions, the conclusion obtained in this work may be inapplicable. For instance [13], Van der Waals force is an unavoidable cohesion force between too fine powders and will increase the value of repose angle. Therefore, for fine powder materials, the weight of Van der Waals force will become greater as the gravity decreases and leads a larger repose angle to the granular pile. Besides, the experimental environment might be another factor affecting the testing results. For the tests of Kleinhans et al. [11] conducted on a parabolic flight, they found that, when the gravity decreased, the static repose angle increased with 5° but the dynamic repose angle decreased with 10°, i.e., the avalanche size becomes greater. The aircraft vibration was an inevitable environment factor and might make a great influence on the powder avalanches. Maybe the role of aircraft became greater when the gravity decreased and thus enhanced the size of powder avalanches.

4. Conclusions

(1) For particles normally distributed or lognormally distributed in size, the effect of the gravitational acceleration on the repose angle of pile is negligible, although gravity is the original driving force for the formation of particulate pile

(2) From the statistical view, for a pile composed with normally distributed particles or lognormally distributed particle, the contact forces within the pile are

linearly proportional to the gravitational acceleration. The ratio between tangential and normal contact forces at contact points of a pile is independent of the gravitational acceleration. This law will not be affected by the size distribution of particles

In some previous literatures, it is found that the repose angle was increased or decreased by a certain extent when the gravity changes. That is entirely opposite to our results that the repose angle is not related to the gravity force. It must be stated that the conclusion of this work is achieved under the ideal condition where just the pure contact force of elastic-plastic deformation between particles was considered. In actual conditions, many other parameters will affect the repose angle of granular pile such as particle shape, roughness of the baseplate, cohesion forces among particles, and testing environment factors. These parameters would make combined effects on the repose angle with the gravity force. And then, the conclusion that the repose angle is independent on the gravity may need an amendment. This issue under more complex conditions will be studied and discussed in our future work.

Data Availability

The original data used to support the findings of this study are available from the corresponding author upon request. Requests for data, 12 months after the publication of this article, will be considered by the corresponding author.

Conflicts of Interest

The authors declare that there is no conflict of interest regarding the publication of this paper.

Acknowledgments

This work was supported by the China Postdoctoral Science Foundation (Grant No.: 2017M622425 and 2018T110756) and the National Natural Science Foundation of China (Grant No.: 51705170).

References

[1] K. E. Ileleji and B. Zhou, "The angle of repose of bulk corn stover particles," *Powder Technology*, vol. 187, no. 2, pp. 110–118, 2008.

[2] K. Taylor, P. J. King, and M. R. Swift, "Influence of magnetic cohesion on the stability of granular slopes," *Physical Review E*, vol. 78, no. 3, article 031304, 2008.

[3] F. Pignatel, C. Asselin, L. Krieger, I. C. Christov, J. M. Ottino, and R. M. Lueptow, "Parameters and scalings for dry and immersed granular flowing layers in rotating tumblers," *Physical Review E*, vol. 86, no. 1, article 011304, 2012.

[4] W. Wang, J. Zhang, S. Yang, H. Zhang, H. Yang, and G. Yue, "Experimental study on the angle of repose of pulverized coal," *Particuology*, vol. 8, no. 5, pp. 482–485, 2010.

[5] F. Pacheco-Vázquez, A. Y. Ramos-Reyes, and S. Hidalgo-Caballero, "Surface depression with double-angle geometry during the discharge of grains from a silo," *Physical Review E*, vol. 96, no. 2, article 022901, 2017.

[6] J. Blum, "Astrophysical microgravity experiments with dust particles," *Microgravity Science and Technology*, vol. 22, no. 4, pp. 517–527, 2010.

[7] S. Silvestro, D. A. Vaz, R. C. Ewing et al., "Pervasive aeolian activity along rover Curiosity's traverse in Gale Crater, Mars," *Geology*, vol. 41, no. 4, pp. 483–486, 2013.

[8] J. Y. Wong, "Predicting the performances of rigid rover wheels on extraterrestrial surfaces based on test results obtained on earth," *Journal of Terramechanics*, vol. 49, no. 1, pp. 49–61, 2012.

[9] A. Brucks, T. Arndt, J. M. Ottino, and R. M. Lueptow, "Behavior of flowing granular materials under variable g," *Physical Review E*, vol. 75, no. 3, article 032301, 2007.

[10] B. H. N. Horgan and J. F. Bell III, "Seasonally active slipface avalanches in the north polar sand sea of Mars: evidence for a wind-related origin," *Geophysical Research Letters*, vol. 39, no. 9, 2012.

[11] M. G. Kleinhans, H. Markies, S. J. de Vet, A. C. in't Veld, and F. N. Postema, "Static and dynamic angles of repose in loose granular materials under reduced gravity," *Journal of Geophysical Research*, vol. 116, no. E11, 2011.

[12] H. Nakashima, Y. Shioji, T. Kobayashi et al., "Determining the angle of repose of sand under low-gravity conditions using discrete element method," *Journal of Terramechanics*, vol. 48, no. 1, pp. 17–26, 2011.

[13] P. G. Hofmeister, J. Blum, and D. Heiβelmann, "The flow of granular matter under reduced-gravity conditions," *AIP Conference Proceedings*, vol. 1145, no. 1, pp. 71–74, 2009.

[14] C. Atwood-Stone and A. S. McEwen, "Avalanche slope angles in low-gravity environments from active Martian sand dunes," *Geophysical Research Letters*, vol. 40, no. 12, pp. 2929–2934, 2013.

[15] S. Ji and H. H. Shen, "Two-dimensional simulation of the angle of repose for a particle system with electrostatic charge under lunar and earth gravity," *Journal of Aerospace Engineering*, vol. 22, no. 1, pp. 10–14, 2009.

[16] H. Chen, Y. L. Liu, X. Q. Zhao, Y. G. Xiao, and Y. Liu, "Numerical investigation on angle of repose and force network from granular pile in variable gravitational environments," *Powder Technology*, vol. 283, pp. 607–617, 2015.

[17] P. A. Cundall and O. D. L. Strack, "A discrete numerical model for granular assemblies," *Geotechnique*, vol. 29, no. 1, pp. 47–65, 1979.

[18] L. Zhang, Y. Wang, and J. Zhang, "Force-chain distributions in granular systems," *Physical Review E*, vol. 89, no. 1, article 012203, 2014.

[19] C. Thornton and Z. Ning, "A theoretical model for the stick/bounce behaviour of adhesive, elastic-plastic spheres," *Powder Technology*, vol. 99, no. 2, pp. 154–162, 1998.

[20] Y. C. Zhou, B. H. Xu, A. B. Yu, and P. Zulli, "Numerical investigation of the angle of repose of monosized spheres," *Physical Review E*, vol. 64, no. 2, article 21301, 2001.

[21] C. O'Sullivan and J. D. Bray, "Selecting a suitable time step for discrete element simulations that use the central difference time integration scheme," *Engineering Computations*, vol. 21, no. 2/3/4, pp. 278–303, 2004.

[22] H. M. Beakawi Al-Hashemi and O. S. Baghabra Al-Amoudi, "A review on the angle of repose of granular materials," *Powder Technology*, vol. 330, pp. 397–417, 2018.